Soft Matter

PAPER

View Article Online
View Journal | View Issue

Cite this: *Soft Matter*, 2014, **10**, 3027

Rheology of soft colloids across the onset of rigidity: scaling behavior, thermal, and non-thermal responses†

Anindita Basu,‡[a] Ye Xu,‡*[ab] Tim Still,[ab] P. E. Arratia,[c] Zexin Zhang,[d] K. N. Nordstrom,[a] Jennifer M. Rieser,[a] J. P. Gollub,[ae] D. J. Durian[a] and A. G. Yodh[a]

Received 18th September 2013
Accepted 24th January 2014

DOI: 10.1039/c3sm52454j

www.rsc.org/softmatter

We study the rheological behavior of colloidal suspensions composed of soft sub-micron-size hydrogel particles across the liquid–solid transition. The measured stress and strain-rate data, when normalized by thermal stress and time scales, suggest our systems reside in a regime wherein thermal effects are important. In a different vein, critical point scaling predictions for the jamming transition, typical in athermal systems, are tested. Near dynamic arrest, the suspensions exhibit scaling exponents similar to those reported in Nordstrom *et al.*, *Phys. Rev. Lett.*, 2010, **105**, 175701. The observation suggests that our system exhibits a glass transition near the onset of rigidity, but it also exhibits a jamming-like scaling further from the transition point. These observations are thought-provoking in light of recent theoretical and simulation findings, which show that suspension rheology across the full range of microgel particle experiments can exhibit both thermal and athermal mechanisms.

1 Introduction

The onset of dynamic arrest associated with the liquid–solid transition is found under a variety of conditions and across a wide range of disordered materials including polymeric glasses,[2] colloidal suspensions,[3–6] granular media,[7] emulsions,[8–12] and foams.[13–15] In a suspension of soft colloidal particles under shear, for example, the onset of solidity is readily observed when a critical volume fraction, ϕ_c, is approached from below. The precise character of this rigidity-onset transition is a topic of current interest whose physics can depend on parameters such as the strength and character of interparticle interactions and the nature of the spatio-temporal fluctuations in the sample.[16–18] For colloidal packings with small and soft particles, the effects of random thermal motion are significant. For granular media, on the other hand, the thermal effects are negligible, but non-thermal fluctuations are often present, and the emergence of solidity depends on particle contacts and particle interactions, among other factors. The concepts of jamming theory have been applied to understand this problem, and collectively this work suggests that the behavior of stress and strain-rate near the jamming point should exhibit critical scaling;[19–25] some of these predictions have been observed in simulation,[19] as well as experimentally in microfluidic rheology measurements of soft colloids.[1] In a different vein, recent simulation work has suggested that two kinds of mechanistic processes can arise in the colloidal rheology experiments; these two types of transitions differ for thermal *versus* non-thermal systems, and they are most easily distinguished when stress and strain-rate are normalized by specific thermal parameters.[16,17] Ultimately, a better understanding of the details of these rigidity-onset phenomena will entail careful experiment and attention to details of the colloidal system, including particle size, stiffness, interaction, and more.

In this paper we take new experimental and analytical steps in this direction. Specifically, we employ both steady-state and frequency-dependent macrorheology to study the shear response of monodisperse and bidisperse colloidal suspensions composed of soft, thermoresponsive poly(*N*-isopropylacrylamide) (PNIPAM) microgel particles. The thermoresponsive microgel particles permit continuous tuning of colloidal volume fraction across ϕ_c.[26–30] Importantly, the size and stiffness of our particular PNIPAM particles are intermediate to those in previous macrorheology work on PNIPAM samples with small particles ($\approx$60–200 nm), wherein thermal effects might be expected to dominate,[30,31] and to those in

[a]*Department of Physics and Astronomy, University of Pennsylvania, Philadelphia, PA 19104, USA. E-mail: yexu@seas.upenn.edu*

[b]*Complex Assemblies of Soft Matter, CNRS-Rhodia-UPenn UMI 3254, Bristol, PA 19007, USA*

[c]*Department of Mechanical Engineering and Applied Mechanics, University of Pennsylvania, Philadelphia, PA 19104, USA*

[d]*Center for Soft Condensed Matter Physics and Interdisciplinary Research, Soochow University, Suzhou, China*

[e]*Department of Physics, Haverford College, PA 19041, USA*

† Electronic supplementary information (ESI) available. See DOI: 10.1039/c3sm52454j

‡ These authors contributed equally to this work.

microfluidic rheology experiments with large PNIPAM particles (>1 μm), wherein thermal effects are much less important.[1]

We observe jamming-like scaling of the suspension for stress *versus* strain-rate data, similar to behaviors found in the steady flow microfluidic rheology measurements[1] and simulation;[19] in particular, the fitted scaling exponents are approximately the same across the two experiments within experimental error. However, the size of the yield stresses observed in our rheometer measurements are approximately one order of magnitude smaller than in the microfluidic rheology experiments,[1] and the size of the strain-rates near ϕ_c differ by approximately two orders of magnitude. These similarities and differences led us to re-examine the full group of microgel particle experiments performed to date, in the context of recent suggestions about how to normalize stress and strain-rate by thermal factors;[16,17] in this context, we find that the different sizes and moduli of the PNIPAM particles lead us to different conclusions about the influence of thermal *versus* non-thermal fluctuations in the respective rheology experiments. Specifically, the normalized data suggest that the larger and harder particles studied with microfluidic rheology[1] probe athermal jamming phenomena, while the experiments reported herein lie in a regime wherein both thermal and non-thermal effects can be important.

2 Materials and methods

2.1 Hydrogel particles

Poly(*N*-isopropylacrylamide), PNIPAM, particles of two different diameters ($D_s \approx 500$ nm and $D_l \approx 700$ nm at 296 K, polydispersity < 0.1) were prepared by radical precipitation polymerization of *N*-isopropylacrylamide, *N*,*N*′-methylenbisacrylamide crosslinker and ammonium persulfate initiator.[32,33] Aqueous suspensions of PNIPAM microspheres with packing fraction $\phi \approx 0.6$ and estimated number density $N \approx 2.6 \times 10^{18}$ m^{-3} were prepared by centrifugation and subsequent dilution. The samples investigated in this paper include a monodisperse suspension of the larger PNIPAM particles and a bidisperse suspension of both species with an approximately equal number ratio. As shown in previous experiments, such PNIPAM particles most likely interact *via* a Hertzian potential.[1,34,35] The elastic moduli of the particles were estimated following a centrifugation procedure introduced previously[36] (see more details in ESI†). The Young's moduli, E, of our PNIPAM particles were estimated to vary between 8 and 25 kPa for temperatures between 291 and 295 K. We note that the particles used herein are about 50% softer than those used at corresponding temperatures in the microfluidics experiments of Nordstrom *et al.*[1] Note that the crosslinking density in PNIPAM particles is not homogeneous, with a high number of cross-links in the center of the particles and much fewer cross-links towards the outer regions.[26] At the compressions investigated in our study, the interaction of touching particles is dominated by the elastic properties of the soft "shells".[37] Note further that in recent publications by Scheffold *et al.*[37] and Romeo and Ciamarra,[38] theoretical models for the concentration-dependence of shear elasticity were developed starting from single particle properties and applied to hydrogel experiments. Future temperature-dependent rheology experiments with PNIPAM particles investigating a much larger range of ϕ–ϕ_J than this study may be utilized to further test these predictions.

2.2 Dynamic light scattering (DLS)

Particle diameter, D, as a function of temperature, T, was measured by dynamic light scattering (Brookhaven Instruments, $\lambda_0 = 632.8$ nm, 15 mV, $\theta = 60°$). Fig. 1a shows the measured particle diameters in the temperature range between 291 K and 309 K. $D(T)$ is essentially linear in this regime.[1] The slopes of these lines were obtained from linear fits to the DLS data for smaller and larger PNIPAM particles and were $dD_s/dT = -10.3 \pm 0.8$ nm K^{-1} and $dD_l/dT = -22.0 \pm 1.4$ nm K^{-1}, respectively. This information enables calculation of the packing fraction of the investigated dense suspensions as a function of T using the following relations:

$$\phi_{\mathrm{mono}}(T) = \phi_c \left(\frac{D_c + \frac{dD}{dT}(T - T_c)}{D_c} \right)^3 \quad (1)$$

with critical temperature, T_c, corresponding particle diameter at the critical temperature, D_c, and corresponding critical volume fraction, ϕ_c. For the bidisperse case:

$$\phi_{\mathrm{bi}}(T) = \phi_{c,s} \left(\frac{D_{c,s} + \frac{dD_s}{dT}(T - T_c)}{D_{c,s}} \right)^3 + \phi_{c,l} \left(\frac{D_{c,l} + \frac{dD_l}{dT}(T - T_c)}{D_{c,l}} \right)^3 \quad (2)$$

with $\phi_{c,s} = \phi_c n_s {D_{c,s}}^3 / (n_s {D_{c,s}}^3 + (1 - n_s){D_{c,l}}^3)$ and $\phi_{c,l} = \phi_c - \phi_{c,s}$ being the portions of the critical packing fraction occupied by the small or large particles, respectively. Here n_s is the number fraction of small particles in the sample. In our case, $n_s \approx 0.5$. In our rheology experiments, temperature is the only control parameter, and the critical temperature, T_c, is readily identified as the temperature at which the yield stress becomes finite;

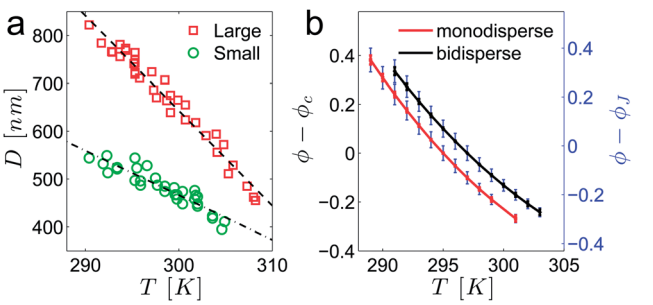

Fig. 1 (a) Hydrodynamic particle diameter, D, as a function of temperature T. Dashed lines are linear fits. (b) $\phi - \phi_c$ and $\phi - \phi_J$ as a function of T using eqn (1) for the monodisperse (large particles) suspension and eqn (2) for the bidisperse (large and small particles) suspensions, assuming $\phi_c = 0.61$ and $\phi_J = 0.64$. Error bars in black and red for $\phi - \phi_c$ when $\phi_c = 0.58$–0.64, and error bars in blue are for $\phi - \phi_J$ for the same range of ϕ_c.

again, $D_c = D(T_c)$ is the particle diameter measured at the critical temperature (Fig. 1a).

Therefore, the only unknown in eqn (1) and (2) is the critical packing fraction, ϕ_c, which we define empirically as the packing fraction when solidification occurs. Note that for different physical scenarios, different ϕ_c are expected. For example, hard thermal particles undergo a colloidal glass transition at $\phi_c \geq 0.58$, whereas the athermal jamming transition occurs at random close packing, *i.e.*, $\phi_J \approx 0.64$. Soft particles at finite temperature, such as those investigated in this study, are expected to undergo a liquid-to-solid transition at packing fractions between these limiting values.

Importantly, many of the major conclusions in this paper are based on scaling laws that depend on the difference, $\phi - \phi_J$ or $\phi - \phi_c$. Note, ϕ_c and ϕ_J need not be the same. For soft particles, a colloidal glass transition can be responsible for the onset of rigidity, and for our particular particles, ϕ_c is expected to 0.61 ± 0.02.[16] Therefore, when plotting $\phi(T) - \phi_c$ in Fig. 1b, we adopt the reasonable assumption that $\phi_c \approx 0.61 \approx \phi_J - 0.03$, slightly below the value of random close packing fraction in three-dimension.[1,39] It is also evident from eqn (1) that $\phi - \phi_c \propto \phi_c$, therefore, small uncertainties in the absolute value of ϕ_c should lead only to small errors in the calculated $\phi(T) - \phi_c$. In order to demonstrate the weak dependency of $\phi(T) - \phi_c$ from the actual value of ϕ_c, we compute the deviations that occur if we assume ϕ_c to be 0.58 or 0.64, respectively; these deviations correspond to the width of error bars in Fig. 1b. Thus, the uncertainty in $\phi(T) - \phi_c$ is small, even when we do not know the exact value of ϕ_c.

2.3 Rheology

The mechanical responses of these suspensions were measured in an AR-G2 rheometer capable of independent stress and strain measurements (TA Instruments), with 4°/40 mm cone-and-plate geometry. Sample temperature was controlled and measured by a Peltier unit and a thermocouple built into the rheometer. A solvent trap was used to prevent sample evaporation during the experiment. The experiments were performed under steady as well as oscillatory shear conditions in order to study both steady-state and frequency-dependent responses. For the range of stresses measured in these experiments, the material density of the PNIPAM microgel particles remains constant at any given temperature, even though their polymer network structure may become deformed.[1,36] Under steady shear, shear stress (σ) *versus* strain-rate ($\dot{\gamma}$) data were obtained as a function of $\phi - \phi_c$. Similarly, shear elastic (G') and viscous (G'') moduli were recorded as a function of oscillatory frequency (ω) across the liquid–solid transition. All oscillatory measurements were carried out in the linear elastic strain regime, wherein the maximum strain amplitude is 2% or less. Special care was taken to restrict all data-sets to low Reynolds numbers (Re = 0.5). By restricting $\dot{\gamma}$ and ω to low values, we ensured that laminar flow conditions were maintained.[40,41] We note that Re < 0.5 is approached at maximum shear rate ($\dot{\gamma} = 10\ s^{-1}$) for liquid-like samples. However, Re is still far less than 0.5 for solid-like samples due to their higher effective viscosity.

We explored the possibility that wall-slip could have a significant effect for the samples and flow regimes studied.[42,43] These test measurements involved a set of control experiments performed using the same instrument with identical plate geometry. In particular, the effect of rheometer surface roughness was checked by performing control experiments with and without roughening the rheometer cone and plate for PNIPAM suspensions with $\phi - \phi_c$ ranging between −0.19 and 0.23 (see ESI†). The control experiments suggest that, for the flow regimes we use, surface roughness has small effect on the resulting steady-state rheology data.

Another potential systematic error that we attempted to avert concerns the effects of shear history. Because PNIPAM particles deswell isotropically with increasing temperature, the samples were always tested starting from low temperature and working to high temperature; in this way any shear history *between* different volume fractions was effectively erased.[6] Further, for measurements at the same temperature, we performed a set of control experiments with and without pre-shear. The results suggest that the same steady-state is reached for each strain-rate (for shearing times of ≈25–30 s used in our experiment), independent of the shear history (see ESI†).

3 Results and discussion

3.1 Steady shear data

Stress (σ) *versus* strain rate ($\dot{\gamma}$) data curves for monodisperse and bidisperse samples are plotted across the liquid-to-solid transition in Fig. 2. The onset of a finite yield stress can be readily identified at $T_c = 295 \pm 1$ K and $T_c = 297 \pm 1$ K for monodisperse and bidisperse samples, respectively. Rheological data in the solid regime can be fit (dashed lines) to the well-known Herschel–Bulkley (HB) phenomenological model:[44,45] $\sigma = \sigma_y + k\dot{\gamma}^n$. Here σ_y is the yield stress, k is a material-dependent constant, and n is the HB scaling exponent. The HB model is commonly used for capturing the non-Newtonian behaviors of colloidal suspensions with strain-rate-dependent viscosity.[46,47] The exponent, n is approximately 1/2 for our solid data: $n \approx 0.50 \pm 0.02$ for the monodisperse PNIPAM system, and $n \approx 0.48 \pm 0.01$ for the bidisperse system.

The stress *vs.* strain-rate curves in Fig. 2 exhibit general features that are similar to those measured in previous microfluidic rheology experiments.[1] Therefore, we first fit our rheological data to predicted critical scaling functions[19] that were employed in Nordstrom *et al.*[1] Specifically, the dimensionless stress, σ/E, and strain rate, $\dot{\gamma}\eta_s/E$, when scaled as $\sigma/E|\phi - \phi_J|^{\Delta}$ and $\dot{\gamma}\eta_s/E|\phi - \phi_J|^{\Gamma}$, were predicted to collapse onto two distinct curves, one above and one below the liquid–solid transition. Here, E is the Young's modulus of PNIPAM particles, η_s is the viscosity of the solvent, and Δ and Γ are scaling parameters. The value of Δ is related to the interparticle potentials and is predict as $\Delta = \alpha - 1/2$, where $\alpha = 5/2$ for particles with Hertzian potentials. It is also predicted that $\beta \equiv \Delta/\Gamma$ should recover the value of HB scaling exponent, n. The differences $|\phi - \phi_J|$ were calculated from eqn (1) and (2) with $T_c = 295 \pm 1$ K (monodisperse) and $T_c = 297 \pm 1$ K (bidisperse), respectively. (We demonstrate in the ESI† that these same values for T_c, taken

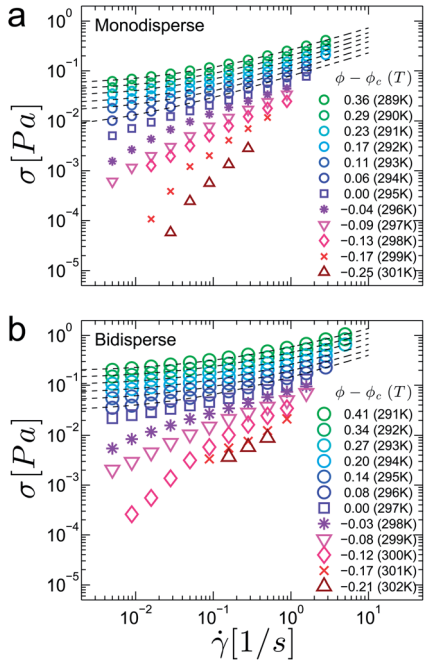

Fig. 2 Stress (σ) *vs.* strain rate ($\dot{\gamma}$) data for aqueous suspensions of (a) monodisperse and (b) bidisperse PNIPAM microgel spheres, obtained using bulk rheology. Each curve is obtained at a different temperature corresponding to a different volume fraction, $\phi - \phi_c$. Dashed lines are Herschel–Bulkley best-fits to the data in the solid regime.

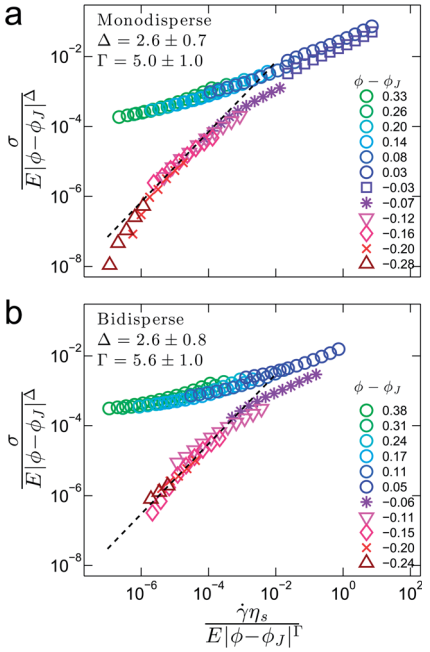

Fig. 3 σ *vs.* $\dot{\gamma}$ for aqueous suspensions of (a) monodisperse and (b) bidisperse PNIPAM microgel spheres scaled with $|\phi - \phi_c|^{\Delta}$ and $|\phi - \phi_c|^{\Gamma}$, respectively. Best-fit values of Δ and Γ are given inside the figures. The dashed lines indicate slopes of unity.

here from the onset of a finite yield stress, are also obtained as fit parameters from a more comprehensive fitting procedure.)

The best-fit scaling exponents, Δ and Γ, are deduced by finding the best collapse of the data onto the two separate branches *above* and *below* the transition. To this end we employed a minimum mean square error (χ^2) fit procedure, analyzing data in discrete steps of 0.1 in Δ and Γ. The best-fit values of the scaling exponents Δ and Γ obtained in this manner for both the monodisperse and bidisperse PNIPAM systems are summarized in Table 1. Uncertainties in fit parameters are determined conservatively for each of the three scaling parameters by the difference between their values at the minimum and their values when χ^2 is increased by a multiplicative factor of two. We see that the fits capture scaling collapse of the experimental data over many orders of magnitude around the liquid-to-solid transition in both the monodisperse and bidisperse suspensions. These high quality fits of solid-like and liquid-like branches are shown in Fig. 3.

We note that the collapsed stress *vs.* strain-rate plots closely resemble the plots in Nordstrom *et al.* (Fig. 5);[1] however, the liquid-like branches of our data show log–log plot slope values that are close to unity at low shear rates for samples with $-0.19 < \phi - \phi_c < 0$ (dashed lines in Fig. 3), and therefore the present samples exhibit more Newtonian-like behavior in the liquid region than the samples in Nordstrom *et al.*,[1] where the log–log slope was approximately 0.5. Finally, we note that values of $\beta \equiv \Delta/\Gamma \sim 0.5$ are obtained using the χ^2-minimization method and are consistent with the Herschel–Bulkley fitting exponent, $n \approx 0.5$, obtained from fitting the rheology data of all PNIPAM suspensions in the solid region (see details in the ESI†).

In short, our rheological data collapses well onto two branches, and good agreement is found between our values for the scaling exponents and those measured for PNIPAM particles[1,19] and for emulsions[12] undergoing a jamming transition. In particular, for jamming, scaling arguments predict that $\Delta = \alpha - 1/2$ with $\alpha = 5/2$ for Hertzian interparticle potentials.[1,24] We find that $\Delta \approx 2.5$ and $\Gamma \approx 5.0$ for both monodisperse and bidisperse PNIPAM systems. Although the values of Δ and Γ are slightly larger than predicted, within the error bars they are the same of those reported for jammed systems. This scaling could be the signature of a jamming-like transition.[48] Note also, our values for $|\phi - \phi_J|$ are mostly of order of 0.1 and are therefore relatively far from the critical point. Many simulation studies of athermal jammed systems have found good fits to single power-law scaling for $|\phi - \phi_J|$ up to order of 0.1;[39,49–51] on the other hand, Olsson and Teitel[20] specifically explored the corrections to the scaling and found the range of $|\phi - \phi_J|$ for critical scaling to be smaller. Our experimental scaling exponents suggest the interpretation of jamming-like scaling, but the limited range of $|\phi - \phi_J|$ precludes an unambiguous conclusion.

Table 1 Critical scaling exponents for viscometry shear data around the fluid–solid transition. Scaling exponents around jamming transition from Nordstrom *et al.*[1] are given for comparison

Sample	Δ	Γ	$\beta = \Delta/\Gamma$
Monodisperse	2.6 ± 0.7	5.0 ± 1.0	0.52 ± 0.16
Bidisperse	2.6 ± 0.8	5.6 ± 1.0	0.46 ± 0.17
Jamming[1]	2.1 ± 0.4	4.1 ± 0.6	0.48 ± 0.03

Although the scaling of our rheometer data closely resembles the scaling behaviors observed in the microfluidic rheological measurements, the measured yield stresses, σ_y, near the transition in Fig. 2a are of order 0.1 Pa, about one order of magnitude lower than those measured with the microfluidic rheological setup. Moreover, the strain rate, $\dot{\gamma}_c$, at which the curves just below and just above ϕ_c collapse, is approximately two orders of magnitude smaller in the macrorheology experiment ($\dot{\gamma}_c \approx 0.1\ s^{-1}$) than in the microfluidic experiment ($\dot{\gamma}_c \approx 10\ s^{-1}$).

To ascertain the possible origin of these differences, we re-analyze these and other microgel-particle rheology data in the context of recent theory and simulation work that explore thermal and non-thermal contributions to the rheological properties of colloidal suspensions.[16–18] The first change of variable of this approach normalizes the measured stress by the thermal stress of the concentrated suspension, *i.e.*, by $\sigma_T = k_BT/D^3$. The second change of variable replaces the strain rate with dimensionless Péclet number, $Pe = \dot{\gamma}\tau_T = \dot{\gamma} \times 3\pi\eta_s D^3/k_BT$, where k_B is Boltzmann's constant, and η_s is the viscosity of the solvent. Similar normalizations were applied in earlier studies investigating the colloidal glass transition.[30] Note that for both normalizations, the particle size contributes as D^3. Therefore, the measurements might be expected to be very sensitive to the particle size: a slight difference in particle size can produce significantly different rheological behaviors. The resultant normalized data curves for both the rheometric experiment and the microfluidic experiment are shown in Fig. 4a and b, respectively. Notice, the normalized shear stresses near the liquid–solid transition in the present experiments are close to unity, while those values in the experiments of Nordstrom *et al.*[1] are at the order of 10^2. Evidently, the two experiments probe very different regions of the rescaled stress/strain-rate diagram, although the overall features look very similar.

Next we consider the strength of the particle interactions compared to thermal energies. Recent simulation work by Ikeda *et al.*[16,17] suggests that under shear, the nature of the liquid–solid transition depends strongly on temperature and particle softness.[16,17] To be precise, it depends on the so-called reduced temperature k_BT/ε, where ε corresponds to the stiffness of the short-range repulsive interaction potential between two particles. For example, in our systems the interaction potential for contacting frictionless spheres is typically assumed to have the form $V(r_{ij}) = (\varepsilon/a)(1 - r_{ij}/\sigma_{ij})^a$ for $r_{ij} < D$, where r_{ij} is the inter-particle distance; $a = 5/2$ for Hertzian interactions.

If we assume our particles interact *via* Hertzian interactions, then it can be readily shown that $\varepsilon = ED^3/[3(1-\nu^2)]$, where E and ν are the Young's modulus and Poisson's ratio of individual PNIPAM particles, respectively.[36,52] For the 500 nm PNIPAM particles used in this paper, we measured $E \approx 5$–25 kPa and $d \approx 0.4$–0.6 μm; for the particles used in Nordstrom *et al.*,[1] the measured $E \approx 10$–50 kPa and $d \approx 1.3$–1.8 μm. Taking $\nu = 0.5$, at the temperatures close to ϕ_c, the particles used in this paper have $k_BT/\varepsilon \approx 5 \times 10^{-6}$, but those used in Nordstrom *et al.*[1] have $k_BT/\varepsilon \approx 10^{-7}$, much closer to the athermal limit where $k_BT/\varepsilon \to 0$. In addition, the stress/strain-rate data in Fig. 4a for the sample with $k_BT/\varepsilon \approx 5 \times 10^{-6}$, probes a region wherein

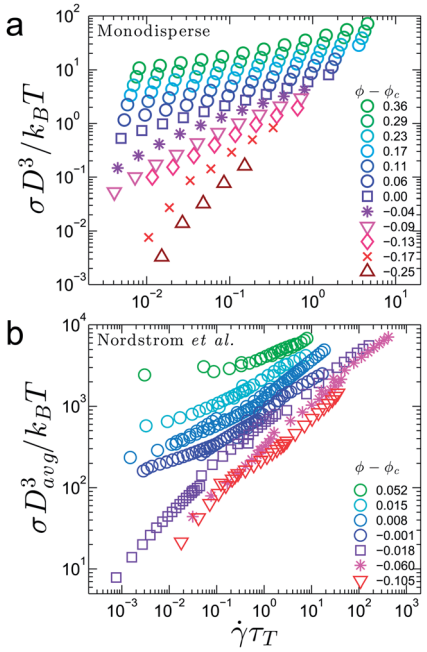

Fig. 4 Rescaled stress/strain-rate data sets reproduced from (a) Fig. 2a and (b) Nordstrom *et al.* (Fig. 3),[1] respectively. Stress is rescaled by the thermal stress scale (D^3/k_BT), and strain-rate is rescaled using the thermal time scale (τ_T) as described in the main text.

$\sigma_y/\sigma_T \approx 1$ and $\dot{\gamma}_c\tau_T \approx 1$, and thus it should be significantly influenced by thermal fluctuations. Therefore, the transition observed in the present experiment is akin to a rheological glass transition. By contrast, the suspensions in the microfluidic experiment, with $k_BT/\varepsilon \approx 10^{-7}$ and whose data is shown in Fig. 4b, probes a substantial region wherein $\sigma_y/\sigma_T \gg 1$ and $\dot{\gamma}_c\tau_T > 1$; thus the corresponding sample behaviors are strongly athermal, and the transition is akin to a jamming transition. We note that this is in contrast to the conclusion in Ikeda *et al.*,[17] where it was suggested that the thermal effect was significant in particle suspensions in Nordstrom *et al.*;[1] this conclusion, however, relied on a different value of ε which was taken from Chen *et al.*[4] We surmise that its high yield stress (in absolute terms) at the liquid–solid transition arises from strong athermally-driven mechanical interactions between colloidal particles, as suggested by this theoretical framework.

To summarize, we test our rheological data against critical scaling models characteristics of jamming theory,[19,21–25] and we find that our systems exhibit some of the signatures of jamming-like scaling. However, mainly as a result of differences in elastic modulus, E, and particle size ($\varepsilon \propto D^3$), the absolute stresses and corresponding strain-rates at ϕ_c are different for the different soft PNIPAM particle suspensions, and these differences appear to be due to the thermal *versus* non-thermal character of the suspensions.[16,17,48]

In other words, the suspensions appear to undergo a glass transition, and, within experimental signal-to-noise, they exhibit jamming-like scaling for $|\phi - \phi_J| \gg 0$. We note that these two conclusions are not necessarily mutually exclusive. Wang and Xu[48] have shown in simulations, for example, that

soft packings at low finite temperature can undergo a colloidal glass transition, leading to the onset of rigidity as a result of kinetic arrest; upon further increase of ϕ, above the isostatic point, they found that jamming-like scaling can be recovered. Unfortunately, because we probe a wide range of packing fractions with minimum $\Delta\phi \approx 0.05$, the present experiments are not optimally sensitized to detect scaling very near the glass transition; nevertheless, a jamming-like scaling fits the experimental data.

These findings can be rationalized when we consider the expected limits of application of jamming-like scaling. Jamming theory is valid for systems at finite temperature T, as long as $T < T^*$, where T^* is a critical temperature. For Hertzian particles, one expects $k_B T^*/\varepsilon_{eff} \propto \alpha(\phi - \phi_J)^2$,[35] where $\varepsilon_{eff} = \varepsilon(\phi - \phi_J)^{1/2}$. The prefactor α is unknown for Hertzian particles, but should be of the same order of magnitude as for harmonic particles, *i.e.*, $\alpha \approx 0.1$.[16,53] For our particles, $\varepsilon \approx 10^5\ k_B T$, and we find $T/T^* \approx 10^4(\phi - \phi_J)^{5/2}$. In other words, $T < T^*$ for $\phi - \phi_J \gtrsim 0.03$, *i.e.*, all of our data (except maybe one) fulfill the condition for jamming-like scaling.

Interestingly, with respect to the signature of glass and jamming transitions, the findings of the simulation work,[16,17] suggest that it may be possible to observe both thermal and non-thermal transitions in the same experimental system if the factor $k_B T/\varepsilon$ can be appropriately tuned and if a wide range of $\dot{\gamma}$ can be experimentally accessed. Future work is needed to further explore these fascinating questions.

3.2 Frequency-dependent rheology

An advantage of our conventional rheometry approach compared to microfluidic measurements is the possibility to test the elastic response in frequency-dependent experiments. In particular, we measure the storage (G') and loss (G'') moduli of the monodisperse and bidisperse PNIPAM systems as a function of oscillation frequency, ω, across the liquid-to-solid transition. We then compare the scaling of the static shear modulus, G_0, with packing fraction, $\phi - \phi_J$, against the scaling predicted for jammed packings of Hertzian spheres.[39,51] As before, the temperature of these systems is systematically varied to change volume fraction, ϕ; thus we obtain G' and G'' as a function of $\phi - \phi_J$ and ω. Fig. 5 shows G' and G'' of monodisperse (a), and bidisperse (b) PNIPAM suspensions as function of ω, and for a range of $\phi - \phi_J > 0$, *i.e.*, in the solid regime. (Note, the maximum applied strain amplitude was $\gamma \leq 0.01$, wherein the response to oscillatory shear is strictly linear, and all measurements are restricted to the laminar flow regime (*i.e.*, Re < 0.1).)

The static shear modulus, G_0, may be extracted from a fitting of the frequency-dependent function $G^* = G_0(1 + \sqrt{i\omega/\omega_n})$,[14,54] where $G^* = G' + iG''$, and where G_0 and characteristic frequency, ω_n, are fitting parameters. In particular, G' and G'' are fit to the following functional forms: $G' = G_0(1 + \sqrt{\omega/(2\omega_n)})$, and $G'' = G_0(\sqrt{\omega/(2\omega_n)})$. These fits are shown in Fig. 5, where the solid lines indicate G' fits and the dashed lines indicate the fits to G''. The quality of the G' fits are high for both monodisperse and bidisperse data-sets over the entire range of frequencies

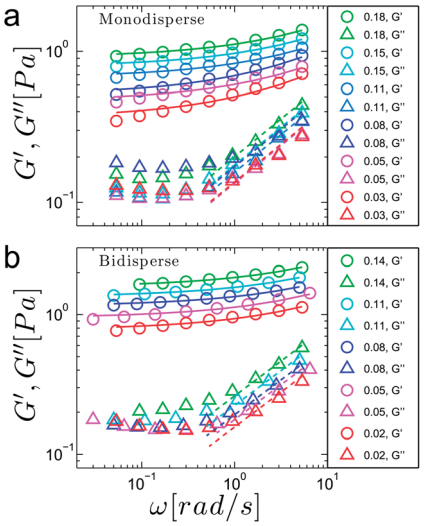

Fig. 5 G' and G'' as function of ω, for aqueous suspensions of (a) monodisperse and (b) bidisperse PNIPAM microgel spheres. Data are obtained applying a maximum strain amplitude of $\gamma = 0.01$. $\phi - \phi_J$ corresponds to temperature steps of 0.5 K (*cf.* Fig. 1). The data are fit to $G' = G_0(1 + \sqrt{\omega/(2\omega_n)})$ (solid lines), and $G'' = G_0(\sqrt{\omega/(2\omega_n)})$ (dashed lines), where G_0, and ω_n are fitting parameters.

shown in the figure. G'', by contrast, is well-approximated by the equation only for $\omega \geq 0.4$ rad s^{-1}. The upturn in G'' for $\omega < 0.4$ rad s^{-1}, is indicative of relaxation[8,45,55] and is not well captured by the fitting form used here.

O'Hern *et al.*[39,51] predicted that G_0 of systems above the jamming transition should scale with $|\phi - \phi_J|$, according to following relation: $G_0 \propto |\phi - \phi_J|^{(\alpha - 1/2)/2}$, where $\alpha = 5/2$ for particles with Hertzian interactions. That is, we expect a linear scaling with $|\phi - \phi_J|$ for Hertzian particles. The experimental G_0, normalized by E, are plotted as a function of $\phi - \phi_J$ in Fig. 6 for the monodisperse and bidisperse samples. Solid lines are linear fits to the data, showing that, once again, the experimental results in our disordered colloidal packings are in reasonable agreement with the scaling predictions made for jammed systems.

Recent calculations by Tighe[25] predict critical scaling behavior of G' and G'' as a function of ω for the jammed systems. In particular, for Hertzian particles, a scaling collapse of G' and G'' *versus* ω is predicted when the moduli are scaled by $|Z - Z_c|^2$ and ω is scaled by $|Z - Z_c|^2$ or $|Z - Z_c|^3$, depending on whether the damping mechanism is dominated by the drag force of the solvent or the viscoelastic Hertzian contacts of particles. Here Z is the average coordination number of the interacting particles, and Z_c is the critical co-ordination number at the jamming transition, when isostaticity is just reached. We experimentally explored the scaling collapse of the oscillatory data using glassy PNIPAM suspensions. Because $|Z - Z_c|$ cannot be measured directly in our experiment, however, we use the relation, $|Z - Z_c| \sim |\phi - \phi_J|^{1/2}$; this relation was first shown in simulations with 2D harmonically repulsive disks near the jamming transition.[49,50] It was also observed in simulations[51] in 3D systems with Hertzian potentials and theoretically studied by Wyart *et al.*[56] Later experiments with 2D photoelastic

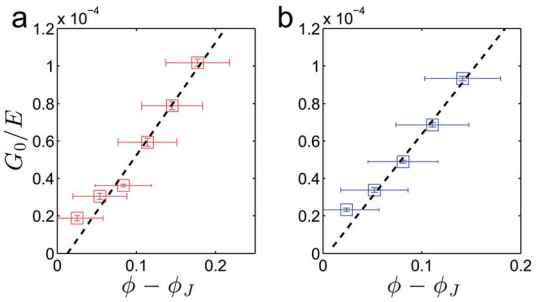

Fig. 6 Dimensionless static shear modulus, G_0/E *vs.* $|\phi - \phi_J|$ for aqueous suspensions of (a) monodisperse and (b) bidisperse PNIPAM particles. The error bars for $\phi - \phi_J$ are derived for uncertainty of $\phi_c = 0.58–0.64$. Dashed lines are best linear fits expected for Hertzian particles ($\alpha = 5/2$).

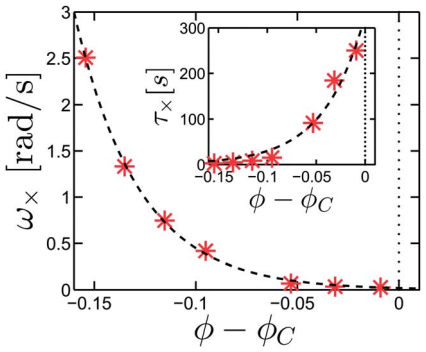

Fig. 8 G' and G'' cross-over frequency, $\omega_\times$ as a function of $\phi - \phi_c$ at $\phi - \phi_c < 0$. Inset: corresponding time scale, $\tau_\times$, *versus* $\phi - \phi_c$. Dashed lines indicate exponential fits.

disks[57,58] and 3D emulsions[59] have confirmed this relation. Fig. 7 shows the scaling collapse of G' and G'', scaled by $E|\phi - \phi_J|$, *versus* ω, scaled by $E|\phi - \phi_J|^{3/2}/\eta_s$. We find decent collapse of G' and G'' onto two master curves except for samples with very small $\phi - \phi_J$ (<0.05) and for G'' at the lowest frequencies (*i.e.*, in agreement with the expected relaxation effects already seen in Fig. 5). Through this data collapse, we derive evidence for Tighe's[25] prediction that the scaling of $G^* = G' + iG''$ with $|\phi - \phi_J|$ holds, not just for the quasi-static limit, but for a broad range of frequencies. We note that similarly good scaling collapse was found when ω is scaled by $E|\phi - \phi_J|/\eta_s$ (see details in ESI†). Unfortunately, we cannot unambiguously determine which damping mechanism plays the dominant role in our system.

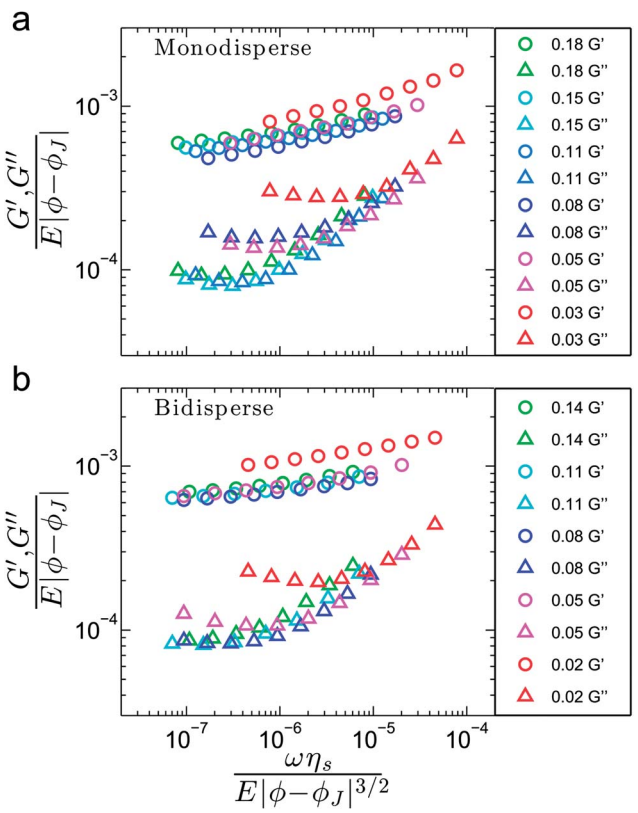

Fig. 7 Volume-fraction-difference-scaled dimensionless moduli, G'/E and G''/E, as function of dimensionless oscillatory frequency, $\omega\eta_s/E$ for (a) monodisperse and (b) bidisperse PNIPAM microgel spheres at $\phi - \phi_J > 0$, assuming Hertzian interactions.

Finally, we measure the cross-over frequency ($\omega_\times$) in the liquid-like suspensions, *i.e.*, for $\phi - \phi_c < 0$. The corresponding time, $\tau_\times = 1/\omega_\times$ indicates the characteristic relaxation time of the system.[55] Fig. 8 plots the $\omega_\times$ *versus* $\phi - \phi_c$ for the bidisperse PNIPAM system (see ESI† for plots of $G'(\omega)$ and $G''(\omega)$ at different $\phi - \phi_c$). $\omega_\times$ and $\tau_\times$ can both be fit well by exponential functions of $\phi - \phi_c$, as indicated by the black dashed lines. At $\phi - \phi_c = -0.01$, for example, $\omega_\times \approx 0.004$ rad s^{-1}, or, alternatively, $\tau_\times \approx 250$ s. Interestingly, this time-scale is of the same order of magnitude as the α-relaxation time reported in a 2D PNIPAM system.[3] Cross-over frequencies measured in the monodisperse PNIPAM system had similar values (data not shown), albeit for the more limited range of $\phi - \phi_c$ investigated.

4 Conclusions

We have investigated both steady-state and frequency-dependent rheological behaviors of 3D monodisperse and bidisperse soft particle colloidal suspensions across the liquid-to-solid transition using macro-rheology. The shear stress *versus* strain-rate curves, for samples far from the liquid–solid transition, exhibit scaling features similar to the critical scaling predictions for jammed athermal systems near the critical point, *e.g.* as found in suspension experiments employing a micro-fluidic apparatus.[1] However, the magnitude of the observed stresses were lower for the smaller/softer microgel particles, and the strain-rates at rigidity onset differed substantially, too. The size and stiffness of the individual particles are expected to modulate the importance of thermal fluctuations in rheology experiments.[16,17] For example, while the thermal effects are negligible in suspensions of large/hard particles,[1] thermal contributions can be significant in systems with relatively smaller and softer particles. Our observations of thermal glass transitions and jamming-like scaling is quantitatively consistent with recent simulation results,[16,48] but a full understanding of the

underlying mechanisms will require further theoretical and experimental investigation.

Acknowledgements

We thank B. Tighe, S. Pathak, W. Poon, L. Hough, K. Schweizer, V. Vitelli, Ke Chen, and A. Liu for valuable discussions, and we are grateful to Rhodia-Solvay in Bristol, PA for providing us with access to their AR-G2 rheometer. This work was supported by the NSF DMR12-05463, DMR-1305199, PENN MRSEC DMR11-20901, NASA NNX08AO0G grants. T. S. thanks DAAD for his post-doctoral fellowship.

References

1 K. N. Nordstrom, E. Verneuil, P. E. Arratia, A. Basu, Z. Zhang, A. G. Yodh, J. P. Gollub and D. J. Durian, *Phys. Rev. Lett.*, 2010, **105**, 175701.
2 H.-N. Lee, K. Paeng, S. F. Swallen and M. D. Ediger, *Science*, 2009, **323**, 231–234.
3 Z. Zhang, N. Xu, D. T. N. Chen, P. Yunker, A. M. Alsayed, K. B. Aptowicz, P. Habdas, A. J. Liu, S. R. Nagel and A. G. Yodh, *Nature*, 2009, **459**, 230.
4 K. Chen, W. G. Ellenbroek, Z. Zhang, D. T. N. Chen, P. J. Yunker, S. Henkes, C. Brito, O. Dauchot, W. van Saarloos, A. J. Liu and A. G. Yodh, *Phys. Rev. Lett.*, 2010, **105**, 025501.
5 E. H. Purnomo, D. van den Ende, S. A. Vanapalli and F. Mugele, *Phys. Rev. Lett.*, 2008, **101**, 238301.
6 D. A. Sessoms, I. Bischofberger, L. Cipelletti and V. Trappe, *Philos. Trans. R. Soc., A*, 2009, **367**, 5013–5032.
7 A. S. Keys, A. R. Abate, S. C. Glotzer and D. J. Durian, *Nat. Phys.*, 2007, **3**, 260–264.
8 T. G. Mason, J. Bibette and D. A. Weitz, *Phys. Rev. Lett.*, 1995, **75**, 2051–2054.
9 T. G. Mason, J. Bibette and D. A. Weitz, *J. Colloid Interface Sci.*, 1996, **179**, 439–448.
10 J. Goyon, A. Colin, G. Ovarlez, A. Ajdari and L. Bocquet, *Nature*, 2008, **454**, 84–87.
11 I. Jorjadze, L.-L. Pontani, K. A. Newhall and J. Brujić, *Proc. Natl. Acad. Sci. U. S. A.*, 2011, **108**, 4286–4291.
12 J. Paredes, M. A. J. Michels and D. Bonn, *Phys. Rev. Lett.*, 2013, **111**, 015701.
13 A. Saint-Jalmes and D. J. Durian, *J. Rheol.*, 1999, **43**, 1411–1422.
14 A. D. Gopal and D. J. Durian, *Phys. Rev. Lett.*, 2003, **91**, 188303.
15 G. Katgert and M. van Hecke, *Europhys. Lett.*, 2010, **92**, 34002.
16 A. Ikeda, L. Berthier and P. Sollich, *Phys. Rev. Lett.*, 2012, **109**, 018301.
17 A. Ikeda, L. Berthier and P. Sollich, *Soft Matter*, 2013, **9**, 7669–7683.
18 A. Ikeda, L. Berthier and G. Biroli, *J. Chem. Phys.*, 2013, **138**, 12A507.
19 P. Olsson and S. Teitel, *Phys. Rev. Lett.*, 2007, **99**, 178001.
20 P. Olsson and S. Teitel, *Phys. Rev. E: Stat., Nonlinear, Soft Matter Phys.*, 2011, **83**, 030302.
21 P. Olsson and S. Teitel, *Phys. Rev. Lett.*, 2012, **109**, 108001.
22 T. Hatano, M. Otsuki and S. Sasa, *J. Phys. Soc. Jpn.*, 2007, **76**, 023001.
23 T. Hatano, *J. Phys. Soc. Jpn.*, 2008, **77**, 123002.
24 B. P. Tighe, E. Woldhuis, J. J. C. Remmers, W. van Saarloos and M. van Hecke, *Phys. Rev. Lett.*, 2010, **105**, 088303.
25 B. P. Tighe, *Phys. Rev. Lett.*, 2011, **107**, 158303.
26 H. Senff and W. Richtering, *J. Chem. Phys.*, 1999, **111**, 1705.
27 H. Senff and W. Richtering, *Colloid Polym. Sci.*, 2000, **278**, 830–840.
28 R. Pelton, *Adv. Colloid Interface Sci.*, 2000, **85**, 1–33.
29 A. M. Alsayed, M. F. Islam, J. Zhang, P. J. Collings and A. G. Yodh, *Science*, 2005, **309**, 1207–1210.
30 V. Carrier and G. Petekidis, *J. Rheol.*, 2009, **53**, 245–273.
31 J. J. Crassous, M. Siebenburger, M. Ballauff, M. Drechsler, O. Henrich and M. Fuchs, *J. Chem. Phys.*, 2006, **125**, 204906.
32 R. Pelton and P. Chibante, *Colloids Surf.*, 1986, **20**, 247–256.
33 A. M. Alsayed, Y. Han and A. Yodh, Melting and geometric frustration in temperature-sensitive colloids, in *Microgel Suspensions*, ed. A. Fernandez-Nieves, H. M. Wyss, J. Mattsson and D. A. Weitz, Wiley-VCH, Weinheim, 2011, pp. 229–281.
34 D. T. N. Chen, K. Chen, L. A. Hough, M. F. Islam and A. G. Yodh, *Macromolecules*, 2010, **43**, 2048.
35 T. Still, C. P. Goodrich, K. Chen, P. J. Yunker, S. Schoenholz, A. J. Liu and A. G. Yodh, arXiv, 2013.
36 K. N. Nordstrom, E. Verneuil, W. G. Ellenbroek, T. C. Lubensky, J. P. Gollub and D. J. Durian, *Phys. Rev. E: Stat., Nonlinear, Soft Matter Phys.*, 2010, **82**, 041403.
37 F. Scheffold, P. Díaz-Leyva, M. Reufer, N. B. Braham, I. Lynch and J. L. Harden, *Phys. Rev. Lett.*, 2010, **104**, 128304.
38 G. Romeo and M. P. Ciamarra, *Soft Matter*, 2013, **9**, 5401–5406.
39 C. S. O'Hern, L. E. Silbert, A. J. Liu and S. R. Nagel, *Phys. Rev. E: Stat., Nonlinear, Soft Matter Phys.*, 2003, **68**, 011306.
40 R. B. Bird, W. E. Stewart and E. N. Lightfoot, *Transport Phenomena*, John Wiley & Sons, Inc., 1960.
41 J. Douglas, *Fluid mechanics*, Pearson/Prentice Hall, 2005.
42 S. P. Meeker, R. T. Bonnecaze and M. Cloitre, *Phys. Rev. Lett.*, 2004, **92**, 198302.
43 S. P. Meeker, R. T. Bonnecaze and M. Cloitre, *J. Rheol.*, 2004, **48**, 1295.
44 C. Macosko, *Rheology: Principles, Measurements, and Applications*, Wiley, 1994.
45 J. Mewis and N. Wagner, *Colloidal Suspension Rheology*, Cambridge University Press, 2012.
46 M. Cloitre, R. Borrega, F. Monti and L. Leibler, *Phys. Rev. Lett.*, 2003, **90**, 068303.
47 J. R. Seth, L. Mohan, C. Locatelli-Champagne, M. Cloitre and R. T. Bonnecaze, *Nat. Mater.*, 2011, **10**, 838–843.
48 L. Wang and N. Xu, *Soft Matter*, 2013, **9**, 2475–2483.
49 D. J. Durian, *Phys. Rev. Lett.*, 1995, **75**, 4780–4783.
50 D. J. Durian, *Phys. Rev. E: Stat. Phys., Plasmas, Fluids, Relat. Interdiscip. Top.*, 1997, **55**, 1739–1751.

51 C. S. O'Hern, S. A. Langer, A. J. Liu and S. R. Nagel, *Phys. Rev. Lett.*, 2002, **88**, 075507.
52 L. D. Landau, E. M. Lifshits, A. D. M. Kosevich and L. P. Pitaevskii, *Theory of elasticity*, Pergamon Press, Oxford, New York, 3rd edn, 1986.
53 A. Ikeda, L. Berthier and G. Biroli, *J. Chem. Phys.*, 2013, **138**, 12A507.
54 A. J. Liu, S. Ramaswamy, T. G. Mason, H. Gang and D. A. Weitz, *Phys. Rev. Lett.*, 1996, **76**, 3017–3020.
55 R. Larson, *The Structure and Rheology of Complex Fluids*, OUP, USA, 1999.
56 M. Wyart, S. R. Nagel and T. A. Witten, *Europhys. Lett.*, 2005, 486–492.
57 T. S. Majmudar, M. Sperl, S. Luding and R. P. Behringer, *Phys. Rev. Lett.*, 2007, **98**, 058001.
58 J. Zhang, T. S. Majmudar, M. Sperl and R. P. Behringer, *Soft Matter*, 2010, **6**, 2982–2991.
59 I. Jorjadze, L.-L. Pontani and J. Brujic, *Phys. Rev. Lett.*, 2013, **110**, 048302.